Extreme anisotropy and anomalous transport properties of heavily electron doped $Li_x(NH_3)_yFe_2Se_2$ single crystals

Shanshan Sun (孙珊珊), Shaohua Wang (王少华), Rong Yu (俞榕), and Hechang Lei (雷和畅)*

Department of Physics and Beijing Key Laboratory of Opto-electronic Functional Materials and Micro-nano Devices, Renmin University of China, Beijing 100872, China

(Received 25 April 2017; revised manuscript received 1 July 2017; published 11 August 2017)

We report the growth of heavily electron doped Li-NH_3 intercalated FeSe single crystals that are free of material complexities and allow access to the intrinsic superconducting properties. $Li_x(NH_3)_yFe_2Se_2$ single crystals show extremely large electronic anisotropy in both normal and superconducting states. They also exhibit anomalous transport properties in the normal state, which are believed to possibly be related to the anisotropy of relaxation time and/or temperature-dependent electron carrier concentration. Taking into account the great chemical flexibility of intercalants in the system, our findings provide a platform to understanding the origin of superconductivity in FeSe-related superconductors.

DOI: 10.1103/PhysRevB.96.064512

I. INTRODUCTION

The electronic structure of FeAs-based superconductors (SCs) usually consists of hole pockets near the Brillouin zone center (Γ point) and electron pockets near the Brillouin zone corners (M point) [1]. The electron scattering between the electron and hole pockets gives rise to a sign-change s-wave pairing (denoted by $s^{\pm}$ pairing) [2,3], as proposed by the spin-fluctuation-mediated pairing theory. Such an $s^{\pm}$ pairing is consistent with most experimental observations [4,5]. As for the FeSe-based SCs, experimental evidence suggests a quite similar pairing mechanism for the bulk FeSe and Fe(Te, Se) [6]. However, the discovery of heavily electron doped (HED) FeSe-based SCs, including $A_xFe_{2-y}Se_2$ (A = alkali metals and Tl), monolayer FeSe thin films grown on $SrTiO_3$ (m-FeSe/STO films), and the recently discovered (Li, Fe)OHFeSe (FeSe-11111), raise a great challenge to the aforementioned pairing mechanism. On the one hand, from transport and spectral measurements [7–10], these HED FeSe-based SCs show a significant enhancement of T_c to 30–40 K compared to bulk FeSe at ambient pressure ($T_c \approx 8$ K) [11]. On the other hand, the hole pockets, which are crucial in the above pairing mechanism, are absent in these compounds [7]. Until now, the mechanism of high-T_c superconductivity in these HED FeSe-based SCs has still not been fully settled. An even more severe problem is that the various material complexities in the already limited number of reported compounds make a systematic study of their intrinsic properties difficult. For example, in $A_xFe_{2-y}Se_2$, the superconductivity could be affected by the ordering of Fe vacancies in the concomitant insulating phase with the chemical formula $A_{0.8}Fe_{1.6}Se_2$ [12,13]. In m-FeSe/STO films, the enhancement of T_c from bulk FeSe could be associated with the interface effect [14–16]. With regard to FeSe-11111, the canted antiferromagnetic order in (Li, Fe)OH layers could have some influence on the superconductivity in FeSe layers [10]. Therefore, in order to confirm that high T_c is a universal property of the HED FeSe-based SCs, it is highly desirable to find a compound without any material complexity.

Recently, superconductivity with T_c up to 45 K has been reported in $AM_x(NH_3)_yFe_2Se_2$ (AM = alkali, alkali-earth, and rare-earth metals) [17–22]. In these materials, the Fe vacancies are almost absent in FeSe layers [19,22], and the AM-NH_3 layers do not exhibit magnetic order. Thus, they serve as good model systems to study the superconductivity of HED FeSe-based SCs. But the investigation of their intrinsic physical properties, especially transport properties, is impeded because of various factors, such as the limited size of (00l)-orientated parent FeSe single crystals, the difficulty of complete intercalation of FeSe single crystals at low temperature, and the instability of samples at room temperature.

In this work, we report the successful growth of $Li_x(NH_3)_yFe_2Se_2$ (LiFeSe-122) single crystals and a comprehensive study of their transport properties. We find that the intercalation of Li-NH_3 significantly enlarges the inter-FeSe-layer distance d, leading to an extreme anisotropy of LiFeSe-122 in both normal and superconducting states. Such a large d with weak interlayer interactions suggests that LiFeSe-122 is very two-dimensional (2D)-like and serves as a good reference to m-FeSe/STO films. The dominant electron-type carriers with a rather high concentration confirm its HED feature and suggest that a universal high-T_c superconductivity persists in a rather wide range of carrier-doping concentration in this family of SCs. Moreover, LiFeSe-122 shows anomalous transport properties in the normal state which imply an exotic Fermi surface topology and are possibly related to the anisotropic relaxation time and the temperature dependence of the carrier concentration. Our work is helpful for understanding the underlying pairing mechanism in the HED FeSe-based SCs. It also sheds light on the origin of superconductivity in other iron-based SCs.

II. METHODS

Single crystals of FeSe were grown by a chemical-vapor-transport technique using elemental Fe, Se, and a eutectic mix of chlorine salts. The Fe and Se powders were mixed together with a molar ratio of 1:1 and loaded into silica ampoules.

*Author to whom correspondence should be addressed: hlei@ruc.edu.cn

Then the eutectic flux of $AlCl_3$ and NaCl (=0.52:0.48) was mixed and loaded into the ampoules, which were subsequently evacuated down to 1 Pa and sealed. The ampoules were put into a horizontal furnace and heated with a temperature gradient (high-temperature region: 690 K; low-temperature region: 620 K) for 30 days. Finally, the furnace was shut down, and the ampoules cooled down naturally. The tetragonal crystals can be obtained after being dissolved in distilled water and rinsed in alcohol. The LiFeSe-122 single crystals were synthesized using the low-temperature ammonothermal technique. The FeSe single crystals and pieces of Li metal with a nominal mole ratio of 1:2 as well as a magnetic stirrer were loaded and sealed into a designed high-pressure vessel (25 mL) with a stop valve for evacuating treatment and another one for introducing NH_3. These manipulations were carried out in an argon-filled glove box in order to prevent air and water contamination. Then, the vessel was taken out of the glove box and evacuated down to 1 mPa by a turbo molecular pump. The NH_3 gas was introduced and condensed by cooling the vessel to 238 K for 20 min. After that, the vessel was taken out of the cooling bath and stirred for 2 d at room temperature in order to facilitate the reaction and to improve the homogeneity of intercalation. Crystals with a typical size $2 \times 3 \times 0.05\ \mathrm{mm}^3$ can be obtained after evacuating the NH_3 gas. X-ray diffraction (XRD) patterns were collected using a Bruker D8 x-ray diffractometer with Cu K_α radiation ($\lambda = 0.15418$ nm) at room temperature. The elemental analysis was performed using inductively coupled plasma atomic emission spectroscopy (ICP-AES) and energy-dispersive x-ray spectroscopy (EDX) analyses. Electrical transport measurements were carried out in a Quantum Design physical property measurement system (PPMS). The longitudinal and Hall electrical resistivities were measured using a four-probe method on rectangular-shaped single crystals. The current flows in the ab plane of the crystal. The Hall resistivity was obtained from the difference in the transverse resistivity measured at the positive and negative fields in order to remove the longitudinal resistivity contribution due to the voltage probe misalignment, i.e., $\rho_{xy}(\mu_0 H) = [\rho(+\mu_0 H) - \rho(-\mu_0 H)]/2$. The c-axis resistivity $\rho_c(T)$ was measured by attaching current and voltage wires on opposite sides of the platelike crystal (see the Supplemental Material [23]). Magnetization measurements were performed in a Quantum Design magnetic property measurement system (MPMS3).

III. RESULTS

The crystal structure of LiFeSe-122 consists of FeSe and Li-NH_3 layers stacking along the c axis alternatively [inset (b) in Fig. 1(a)]. The space group is $I4/mmm$, and each unit cell contains two FeSe layers, the same as the paramagnetic $K_xFe_{2-y}Se_2$ ($T > T_N$) [12]. The difference is that in $K_xFe_{2-y}Se_2$ the K ions are located at the $2a$ position, but this position is occupied by N atoms in LiFeSe-122, and Li ions are located in the $2b$ and $4c$ positions in the latter. In contrast, the space group of FeSe-11111 is $P4/nmm$, and there is only one layer of FeSe in each unit cell [10]. Moreover, the Li-NH_3 layers in LiFeSe-122 are nonmagnetic, while the (Li, Fe)OH layers in FeSe-11111 are antiferromagnetic. The XRD pattern of a LiFeSe-122 single crystal [Fig. 1(a)] reveals

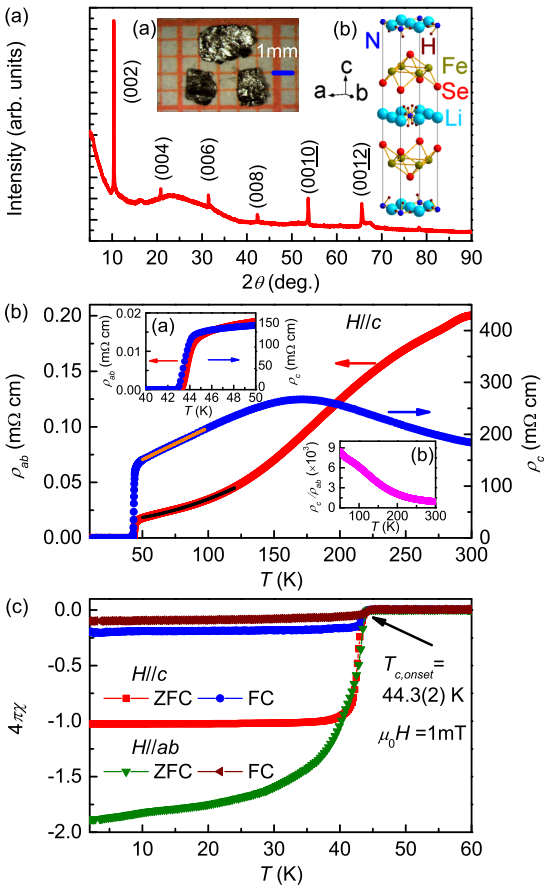

FIG. 1. (a) XRD pattern of a LiFeSe-122 single crystal. Insets (a) and (b) show a photograph and crystal structure of LiFeSe-122 single crystals, respectively. The length of one grid in the photograph is 1 mm. (b) Temperature dependence of in-plane resistivity $\rho_{ab}(T)$ and c-axial resistivity $\rho_c(T)$ at zero field. Insets (a) and (b) show enlarged resistivity curves near T_c and the ratio of ρ_c/ρ_{ab} as a function of temperature, respectively. (c) Temperature dependence of dc magnetic susceptibility $4\pi\chi$ up to 60 K in $\mu_0 H = 1$ mT for $H \parallel c$ and $H \parallel ab$ with ZFC and FC modes.

that the crystal surface is parallel to the $(00l)$ plane and the diffraction peaks shift to lower angles compared to the FeSe single crystal (see the Supplemental Material [23]). The thin platelike crystal with a square shape [inset (a) in Fig. 1(a)] is consistent with the layered structure of LiFeSe-122. The refined a- and c-axial lattice constants using the powder XRD pattern (see the Supplemental Material [23]) are 3.7704(6) and 16.973(7) Å, respectively, consistent with previously reported values [18,20,22]. The a-axial lattice constant is close to that of the bulk FeSe (3.76 Å) [11], suggesting that the intercalation of Li-NH_3 rarely changes the in-plane chemical environment of the FeSe layers [22]. In contrast, the distance d between two adjacent FeSe layers (~8.487 Å, half of the c-axial lattice constant) is much larger than that of bulk FeSe (5.48 Å) [11] but somewhat smaller than that of FeSe-11111 (9.16 Å) [10]. This implies a rather weak interaction between the two adjacent FeSe layers, similar to FeSe-11111. Such weak inter-FeSe-layer bonding is also evidenced by the easy cleavage of crystals along the ab

plane. The atomic ratio of Li:Fe:Se determined from the ICP-AES analysis is 0.18:1:0.9, and the measurement of EDX by examining multiple points on the crystals gives Fe:Se = 0.987:1 (see the Supplemental Material [23]). The slight difference in the Fe:Se ratio determined from ICP and EDX could be due to the different element sensitivities in the two techniques. Nonetheless, the close Fe:Se ratio clearly indicates the absence of Fe vacancies in LiFeSe-122 crystals. The chemical formula is then estimated to be $Li_{0.36}(NH_3)_yFe_2Se_2$, from which an electron doping level of ~0.18 e/Fe is inferred.

Figure 1(b) shows the temperature dependence of in-plane resistivity $\rho_{ab}(T)$ and c-axis resistivity $\rho_c(T)$ at zero field from 10 to 300 K. The in-plane resistivity $\rho_{ab}(T)$ exhibits a metallic behavior in the entire measured temperature range, and the residual resistivity ratio (RRR), defined as $\rho_{ab}(300\,\mathrm{K})/\rho_{ab}(50\,\mathrm{K})$, is about 11.2. Between 50 and 120 K, the $\rho_{ab}(T)$ curve can be well fitted using the formula $\rho_{ab}(T) = \rho_0 + AT^{\alpha}$, with $\rho_0 = 13.2(1)\,\mu\Omega\,\mathrm{cm}$, $A = 1.5(1) \times 10^{-3}\ \mu\Omega\,\mathrm{cm\ K^{-2}}$, and $\alpha = 2.07(2)$. When further lowering the temperature, a sharp superconducting transition appears with $T_{c,\mathrm{onset}} = 44.56(4)\,\mathrm{K}$ and $\Delta T_c = 1.1\,\mathrm{K}$ at zero field [inset (a) in Fig. 1(b)]. T_c is significantly higher than that of bulk FeSe (~9 K; see the Supplemental Material [23]). For $\rho_c(T)$, there is a hump in the curve with the peak position located around 170 K; that is, $\rho_c(T)$ shows an insulating behavior for $T > 170\,\mathrm{K}$ and metallic behavior at $T < 170\,\mathrm{K}$. It has to be mentioned that the peak position varies from sample to sample between 120 and 170 K (see the Supplemental Material [23]). Between 50 and 100 K, the temperature dependence of $\rho_c(T)$ is nearly linear, obviously different from that in $\rho_{ab}(T)$. $T_{c,\mathrm{onset}}$ for $\rho_c(T)$ at zero field is 44.1(1) K with $\Delta T_c = 1.2\,\mathrm{K}$, consistent with that of $\rho_{ab}(T)$ [inset (a) in Fig. 1(b)]. The sharp superconducting transitions for both current directions and rather large RRR in $\rho_{ab}(T)$ indicate the high quality of the single crystal. On the other hand, the absolute value of $\rho_c(T)$ is much larger than $\rho_{ab}(T)$ in the normal state. The ratio of ρ_c/ρ_{ab} [inset (b) in Fig. 1(b)] is about 900 at 300 K and gradually increases to about 8000 when temperature is down to 50 K, indicating a significant anisotropy of LiFeSe-122 crystals. Notably, this anisotropy is even larger than that in FeSe-11111, although the former has a slightly smaller d value [24]. This suggests that the inter-FeSe-layer interaction might be even weaker in LiFeSe-122 than in FeSe-11111.

The zero-field-cooling (ZFC) dc magnetic susceptibility $4\pi\chi(T)$ of a LiFeSe-122 single crystal at $\mu_0 H = 1\,\mathrm{mT}$ for $H \parallel c$ and $H \parallel ab$ [Fig. 1(c)] shows that the superconducting shielding emerges at about 44.3(2) K with a rather sharp transition width, consistent with the resistivity results and previous magnetic susceptibility measurements ($T_c \sim 44\,\mathrm{K}$) [17,18,20,22]. After taking into account the demagnetization effect of the crystal, the superconducting volume fractions (SVFs) estimated from the ZFC data are about 100% and 180% for $H \parallel c$ and $H \parallel ab$, respectively, indicating bulk superconductivity in the LiFeSe-122 single crystal. The larger SVF for $H \parallel ab$ may come from the measurement error of the sample size. For field-cooling (FC) $4\pi\chi(T)$ curves, the SVFs are about 20% and 10% for $H \parallel c$ and $H \parallel ab$ at 2 K, implying a rather strong flux pinning effect in the crystal, especially for $H \parallel ab$.

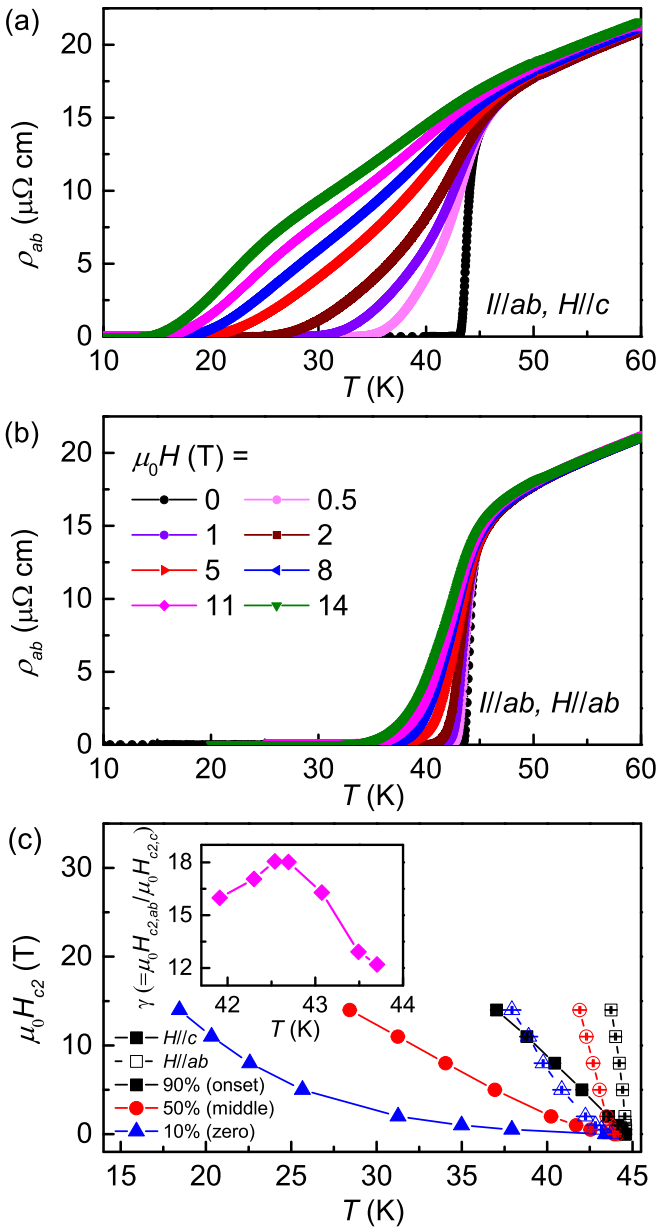

FIG. 2. Temperature dependence of $\rho_{ab}(T)$ at various magnetic fields for (a) $H \parallel ab$ and (b) $H \parallel c$. (c) Temperature dependence of resistive upper critical fields $\mu_0 H_{c2}(T)$ corresponding to three criteria for both field directions. Inset: temperature dependence of the anisotropy of the upper critical field $\gamma = \mu_0 H_{c2,ab}/\mu_0 H_{c2,c}$ using the 50% ρ_n criterion.

Figures 2(a) and 2(b) show the temperature dependence of $\rho_{ab}(T)$ at various magnetic fields up to 14 T for $H \parallel c$ and $H \parallel ab$, respectively. With increasing fields, $T_{c,\mathrm{onset}}$ shifts to lower temperatures only slightly for both field directions. However, the transition width becomes broader at higher fields. The trend is more obvious for $H \parallel c$. Such a resistive tail for $H \parallel c$ has also been observed in $SmFeAsO_{0.85}$ and cuprates [25,26] and suggests the existence of a wide vortex-liquid phase for $H \parallel c$. Interestingly, similar field-induced broadenings of resistive transitions have also been observed in FeSe-11111 [24]. The upper critical fields $\mu_0 H_{c2}(T)$ determined from 90%,

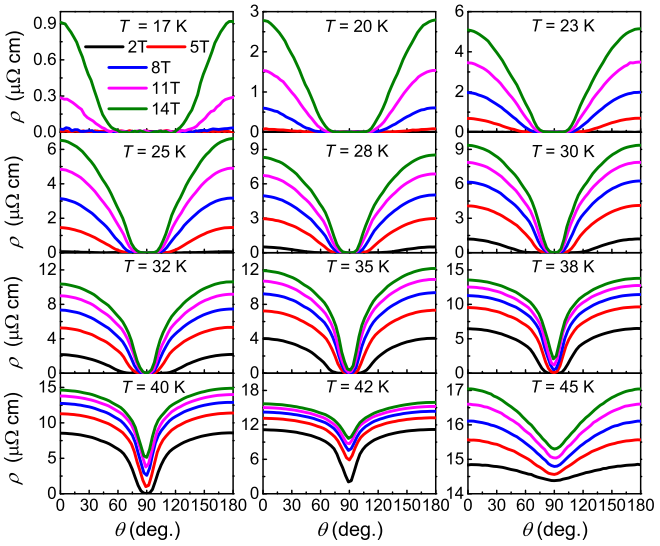

FIG. 3. Angular dependence of in-plane resistivity $\rho_{ab}(\theta,\mu_0 H)$ at various temperatures with $\mu_0 H = 2$, 5, 8, 11, and 14 T.

50%, and 10% ρ_n in Figs. 2(a) and 2(b) are summarized in Fig. 2(c). The $\mu_0 H_{c2}(T)$ curves for $H\|ab$ exhibit larger slopes than those for $H\|c$. Moreover, for $H\|c$, $\mu_0 H_{c2}(T)$ determined from 10% ρ_n is much smaller than those from 50% and 90% ρ_n criteria because the region near 10% ρ_n is related to the vortex-liquid phase, while the region around 90% ρ_n is influenced by superconducting fluctuations. The slopes of $\mu_0 H_{c2}(T)$ near $T_{c,\mathrm{onset}}(0)$, $T_{c,\mathrm{middle}}(0)$, and $T_{c,\mathrm{zero}}(0)$ are -1.86, -0.97, and $-0.16\,\mathrm{T/K}$ for $H\|c$ and -16.19, -6.83, and $-2.45\,\mathrm{T/K}$ for $H\|ab$, respectively. According to the Werthamer-Helfand-Hohenberg formula [27], $\mu_0 H_{c2}(0) = -0.693 T_c (dH_{c2}/dT)\,|_{T_c}$, when choosing the 50% ρ_n criterion, the estimated $\mu_0 H_{c2}(0)$ is 29.5 and 208.7 T for $H\|c$ and $H\|ab$, respectively. The anisotropy of the upper critical field $\gamma = \mu_0 H_{c2,ab}/\mu_0 H_{c2,c}$ is about 12 near $T_{c,\mathrm{middle}}(0)$. It increases to about 18 at 42.6 K and then decreases gradually with decreasing temperature [inset of Fig. 2(c)].

In order to obtain a more accurate value of γ, the angular-resolved in-plane resistivity $\rho_{ab}(\theta,\mu_0 H)$ under various fields at given temperatures has been measured (Fig. 3). All resistivity curves show a symmetric cuplike shape with a minimum value at $\theta = 90^\circ$ and maximum values at $\theta = 0^\circ$ and 180°, where θ is the angle between the direction of the external field and the c axis. This indicates that $\mu_0 H_{c2,ab}$ is larger than $\mu_0 H_{c2,c}$. Moreover, the zero-resistivity region near $\theta = 90^\circ$ becomes narrower with increasing field and temperature. At high temperature (42 and 45 K), the zero-resistivity region disappears in the whole field range. According to the anisotropic Ginzburg-Landau (GL) theory $\mu_0 H_{c2}^{GL}(\theta) = \mu_0 H_{c2,ab}/(\sin^2\theta + \gamma^2\cos^2\theta)^{1/2}$ [28], $\rho_{ab}(\theta,\mu_0 H)$ at a certain temperature under different magnetic fields can be scaled into one curve with a proper anisotropy parameter $\gamma = \mu_0 H_{c2,ab}/\mu_0 H_{c2,c}$. As shown in Fig. 4(a), by adjusting $\gamma(T)$, we obtain very good scaling behaviors for LiFeSe-122 single crystals at various temperatures. The downward trend of $\gamma(T)$ with decreasing temperature is shown in Fig. 4(b) clearly. The values of γ are much larger than those in bulk FeSe [29,30], as well as in most other iron-based SCs [31–33]. However,

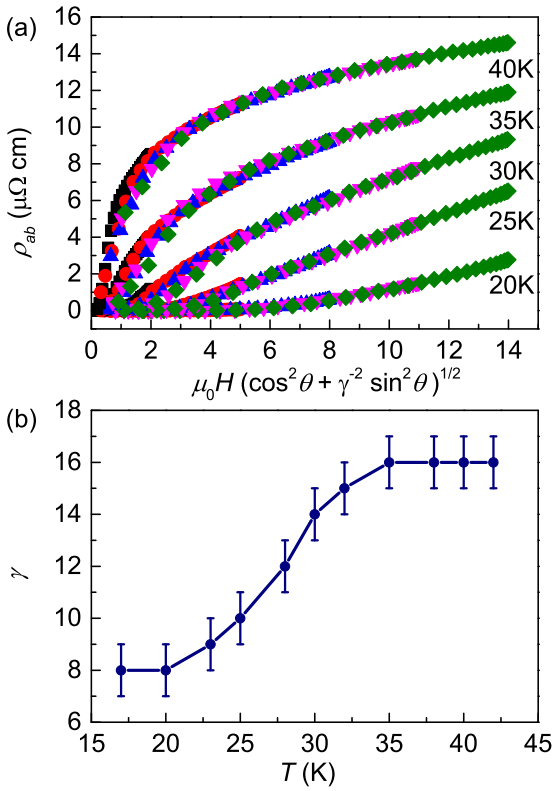

FIG. 4. (a) Scaling behavior of $\rho_{ab}(\theta,\mu_0 H)$ versus $\mu_0 H_s = \mu_0 H(\cos^2\theta + \gamma^2\sin^2\theta)^{1/2}$ from 20 to 40 K at different magnetic fields. (b) Temperature dependence of anisotropy factor γ.

they are comparable to those in FeSe-11111 [34]. According to the GL theory [28], γ is defined by $\sqrt{m_c/m_{ab}}$, where m_c and m_{ab} are the effective masses of electrons along the c axis and ab plane, respectively. The enlarged d in LiFeSe-122 will decrease the interlayer interaction significantly, leading to a quite weak dispersion along the k_z direction [35]. Thus, m_c will become much larger than m_{ab}, and this gives rise to a remarkably large γ in LiFeSe-122. This positive correlation between d and γ near $T_c(0)$ has been observed in many iron-based SCs [36].

The transport properties in the normal state reflect the electronic scattering and can give us information about the Fermi surface (FS), which is important to understanding the superconductivity in iron-based SCs. The inset in Fig. 5(a) shows the magnetoresistance [$\mathrm{MR} = [\rho_{ab}(T,\mu_0 H) - \rho_{ab}(T,0)]/\rho_{ab}(T,0) = \Delta\rho_{ab}/\rho_{ab}(T,0)$] at various temperatures. The MR is relatively small (~6.5% at 50 K and 14 T) and decreases gradually with increasing temperature. Usually, if there is an isotropic relaxation time τ at all points on the FS with a single type of carrier, Kohler's rule will be valid, and the MR at different temperatures can be scaled by the expression $\mathrm{MR} = f(\mu_0 H\tau) = F(\mu_0 H/\rho_{ab}T,0)$ [37]. However, Kohler's rule is clearly violated in the LiFeSe-122 single crystal [Fig. 5(a)]. In general, there are several possibilities leading to the invalidation of Kohler's rule, such as the multiband effect, anisotropic τ, two different relaxation times related to zero-field resistivity and MR, etc. [38]. In order to understand the origin of the violation of Kohler's rule, the temperature dependence of Hall resistivity ρ_{xy} is investigated. ρ_{xy} shows a

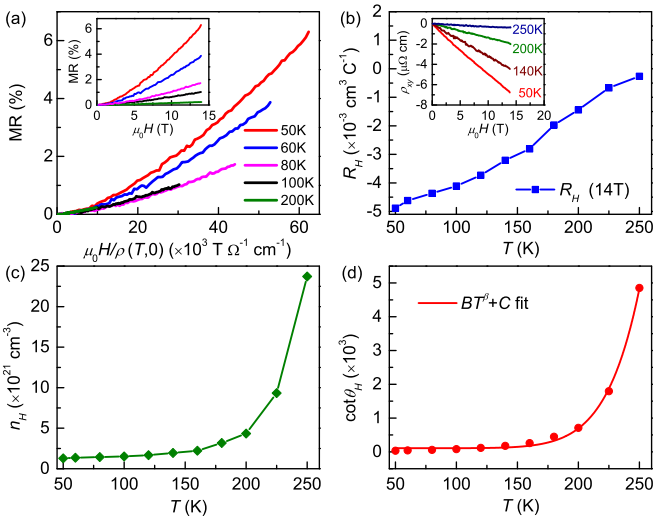

FIG. 5. (a) Kohler plot between 50 and 200 K. Inset: field dependence of MR at different temperatures. (b) Temperature dependence of the Hall coefficient $R_H(T)$ at $\mu_0 H = 14$ T. Inset: field dependence of Hall resistivity ρ_{xy} at various temperatures. (c) Temperature dependence of Hall number $n_H(T) = 1/eR_H$. (d) cotθ_H as a function of temperature. The solid line is the fit using the expression $BT^\beta + C$.

good linear dependence on the magnetic field up to 14 T [inset of Fig. 5(b)], and the Hall coefficient $R_H = \rho_{xy}/\mu_0 H$ at 14 T is negative in the entire temperature range measured [Fig. 5(b)]. This indicates that the dominant carriers are electron type, consistent with the electron doping of Li into FeSe layers. Moreover, the magnitude of R_H reduces with increasing temperature. Strikingly, this temperature dependence and even the absolute value of R_H are quite similar to those in the gated-voltage-modulated FeSe flakes with $T_c = 48$ K [39], strongly suggesting a universal underlying physics in these HED FeSe-based SCs. In contrast, FeSe-11111 exhibits the concave shape of R_H with a characteristic temperature $T^* \sim 120$ K, possibly related to the magnetic properties of (Li, Fe)OH layers that are absent in LiFeSe-122 [24].

The angle-resolved photoemission spectroscopy (ARPES) results show that the hole pockets at the Γ point are absent in most HED FeSe-based SCs, such as (Tl, Rb)$_x$Fe$_{2-y}$Se$_2$, FeSe-11111, and m-FeSe/STO films [7]. A theoretical calculation for LiFeSe-122 also suggests that with electron doping, the size of the hole pockets remarkably shrinks, while the size of the electron pockets around the M point increases [35]. It is then most likely that the electron pockets in LiFeSe-122 play a dominant role in the transport properties in the normal state. As shown in Fig. 5(c), the apparent carrier concentration (i.e., the Hall number $n_H = 1/eR_H$) is weakly temperature dependent below about 180 K, consistent with a single-band model with only electron pockets in LiFeSe-122. The estimated n_H at 50 K is about 1.3×10^{21} cm^{-3}, much larger than that in FeSe [40] but comparable to 3×10^{21} cm^{-3}, a value found by assuming 0.18 electron transferred from Li to each Fe atom. When $T >$ 180 K, n_H increases quickly, implying that other factors may have some influence on n_H, such as the anisotropic relaxation time τ along the FSs with different temperature dependences [38,41], if the shape of the electron pockets of LiFeSe-122 is far from cylindrical [35]. Moreover, n_H could also change at high temperature due to the thermal excitations of carriers among the narrow bands when the Fermi energy E_F is close to the bottom or top of a band [42].

The Hall angle cot$\theta_H = \rho_{xx}/\rho_{xy} \equiv 1/(\omega_c \tau_H)$, where ω_c is the cyclotron frequency and τ_H is the relaxation time determined from the Hall angle, reveals more intrinsic features of the relaxation time. For iron-based SCs, cotθ_H usually follows a phenomenological formula, cot$\theta_H = BT^\beta + C$, with the exponent β being between 2 and 4 [43]. In contrast, cotθ_H of LiFeSe-122 exhibits strong temperature dependence and increases quickly when $T > 180$ K [Fig. 5(d)]. The fit between 50 and 250 K using the above function gives $\beta = 9.3(3)$, which is enormously larger than the value in any other iron-based SC. The origin of such a large β is still unclear, and one possible explanation for the significant enhancement of cotθ_H above 180 K could be the emergence of the multiband effect because of thermal excitations of hole-type carriers at high temperature. Thus, either an anisotropic τ or the multiband behavior at high temperature may lead to the violation of Kohler's rule in LiFeSe-122.

IV. DISCUSSION

The space group of both LiFeSe-122 and K$_x$Fe$_{2-y}$Se$_2$ is $I4/mmm$, while it is $P4/nmm$ for FeSe-11111. It has been argued that this difference results in distinct electronic structures in the two classes of compounds and will strongly affect the pairing symmetry of K$_x$Fe$_{2-y}$Se$_2$ [44]. However, due to material complexity, the pairing symmetry of K$_x$Fe$_{2-y}$Se$_2$ has not been fully settled, although there are already a number of theoretical proposals [45–47]. Given the same structural symmetry and similar electron doping level, we expect studying the superconducting pairing of LiFeSe-122 can solve this open issue. Despite the different lattice structures, both LiFeSe-122 and FeSe-11111 exhibit large anisotropy in both normal and superconducting states, and they have comparable T_c [24]. The electronic anisotropy is likely associated with the very large structural anisotropy (large d values) among the iron-based SCs, which gives rise to a highly 2D electronic structure.

To understand the comparable T_c in LiFeSe-122 and other HED FeSe-based SCs, we summarize the T_c values with the inter-FeSe-layer distance d and the electron doping level in Fig. 6 (data are taken from the literature [7,39,48–51]). A previous study summarizing the relationship between T_c and the d value implies that T_c will increase with increasing d until $d \approx 8.5$ Å, above which T_c saturates [52]. This seems to be valid for most HED FeSe-based SCs [Fig. 6(a)], but a recent work on gated-voltage-modulated FeSe flakes with $T_c^{\text{onset}} \sim 48$ K [emphasized in Fig. 6(a) by the black circle] [39] indicated that the d value may not be a major factor of the enhancement of superconductivity in FeSe-based SCs. More importantly, notice that all high-T_c FeSe-based SCs at ambient pressure with increased d values are HED. The results summarized in Fig. 6(b) indicate that the high-T_c superconductivity emerges and is robust against the size variety of electron pockets once the electron doping level is larger than 0.05 e/Fe. One exception is A$_x$Fe$_{2-y}$Se$_2$, which shows an electron doping level similar to that of LiFeSe-122

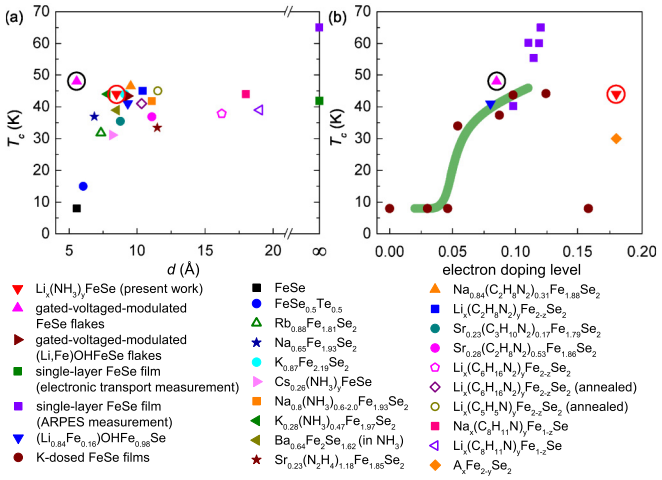

FIG. 6. T_c as a function of (a) d and (b) electron doping level in HED FeSe-based SCs. The results of the present work and gated-voltage-modulated FeSe flakes are emphasized by red and black circles, respectively. The green line in (b) serves as a guide to the eye.

but with much lower T_c (∼30 K) [7]. The existence of Fe vacancies in FeSe layers could be closely related to the suppression of T_c. When the Fe vacancies are ordered in many FeSe-based SCs, such as $Fe_{1-x}Se$ and $K_2Fe_4Se_5$, these compounds become insulators and are regarded as the parent phases of FeSe-based SCs [53,54]. Once the Fe vacancy order is suppressed by either disorder or Fe filling, the superconductivity emerges [54,55]. Furthermore, if the Fe vacancies in $A_xFe_{2-y}Se_2$ are fully filled, another SC phase coexisting with the 30 K SC phase will appear, and T_c will drastically increase to 44 K [56]. This suggests that the Fe vacancies are possibly disadvantageous to superconductivity. As for m-FeSe/STO films, they have the highest T_c, and their carrier doping levels range between those of LiFeSe-122 and FeSe-11111. This implies that either an optimal doping level exists or other factors may influence superconductivity. For example, the interfacial coupling between the FeSe film and the STO substrate could be important to boosting T_c to an unprecedented value [14–16]. In addition, it should be noted that although in bulk FeSe T_c is enhanced to about 38 K after the suppression of nematicity (structural transition), the way to realize comparable T_c values in bulk FeSe and LiFeSe-122 could be very different because of their distinct electronic structures. The transport properties of FeSe under hydrostatic pressures up to 8.8 GPa indicate that the dominant carriers are hole type when the maximum T_c is about 38.3 K, and theoretical calculations imply that both electron and hole pockets exist in the Brillouin zone [57]. These results are different from the case of LiFeSe-122 or any other known HED FeSe-based SC in which the dominant carriers are electron type, associated with the electron pockets near the Brillouin zone corners.

V. CONCLUSION

In summary, we have successfully synthesized HED FeSe-based SC LiFeSe-122 single crystals. Our current observations of a LiFeSe-122 single crystal without materials complexity suggest that the superconductivity in HED FeSe-based SCs is determined mainly by the electron doping level, and in particular, the suppression of hole pockets is intimately related to the giant enhancement of T_c to 40–50 K. Moreover, once above a threshold value (0.05 e/Fe), T_c seems to be insensitive to the carrier concentration and strong anisotropy of τ, i.e., insensitive to the sizes and shapes of electron pockets. These results will impose some constraints on theories. In practice, many kinds of AM as well as organic molecules can be intercalated between FeSe layers, and by carefully choosing suitable combinations of AM and organic molecules, the electron doping level, crystallographic structure, and strength of inter-FeSe-layer coupling can be fine-tuned. Therefore, this superconducting family provides a unique platform for studying the origin of high-T_c superconductivity in FeSe-based SCs.

ACKNOWLEDGMENTS

This work was supported by the Ministry of Science and Technology of China (No. 2016YFA0300504), the National Natural Science Foundation of China (No. 11574394), the Fundamental Research Funds for the Central Universities, and the Research Funds of Renmin University of China (RUC; No. 15XNLF06 and No. 15XNLQ07). R.Y. was supported by the Ministry of Science and Technology of China (No. 2016YFA0300504) and the National Natural Science Foundation of China (No. 11374361 and No. 11674392).

S.S. and S.W. contributed equally to this work.

[1] G. R. Stewart, Superconductivity in iron compounds, Rev. Mod. Phys. **83**, 1589 (2011).

[2] K. Kuroki, S. Onari, R. Arita, H. Usui, Y. Tanaka, H. Kontani, and H. Aoki, Unconventional Pairing Originating from the Disconnected Fermi Surfaces of Superconducting $LaFeAsO_{1-x}F_x$, Phys. Rev. Lett. **101**, 087004 (2008).

[3] I. I. Mazin, D. J. Singh, M. D. Johannes, and M. H. Du, Unconventional Superconductivity with a Sign Reversal in the Order Parameter of $LaFeAsO_{1-x}F_x$, Phys. Rev. Lett. **101**, 057003 (2008).

[4] P. Richard, T. Sato, K. Nakayama, T. Takahashi, and H. Ding, Fe-based superconductors: An angle-resolved photoemission spectroscopy perspective, Rep. Prog. Phys. **74**, 124512 (2011).

[5] P. Dai, Antiferromagnetic order and spin dynamics in iron-based superconductors, Rev. Mod. Phys. **87**, 855 (2015).

[6] X. Liu, L. Zhao, S. L. He, J. F. He, D. F. Liu, D. X. Mou, B. Shen, Y. Hu, J. W. Huang, and X. J. Zhou, Electronic structure and superconductivity of FeSe-related superconductors, J. Phys. Condens. Matter **27**, 183201 (2015).

[7] L. Zhao, A. J. Liang, D. N. Yuan, Y. Hu, D. F. Liu, J. W. Huang, S. L. He, B. Shen, Y. Xu, X. Liu, L. Yu, G. L. Liu, H. X. Zhou, Y. L. Huang, X. L. Dong, F. Zhou, K. Liu, Z. Y. Lu, Z. X. Zhao, C. T. Chen, Z. Y. Xu, and X. J. Zhou, Common electronic origin

of superconductivity in (Li, Fe)OHFeSe bulk superconductor and single-layer FeSe/$SrTiO_3$ films, Nat. Commun. **7**, 10608 (2016).

[8] W. H. Zhang, Y. Sun, J. S. Zhang, F. S. Li, M. H. Guo, Y. F. Zhao, H. M. Zhang, J. P. Peng, Y. Xing, H. C. Wang, T. Fujita, A. Hirata, Z. Li, H. Ding, C. J. Tang, M. Wang, Q. Y. Wang, K. He, S. H. Ji, X. Chen, J. F. Wang, Z. C. Xia, L. Li, Y. Y. Wang, J. Wang, L. L. Wang, M. W. Chen, Q. K. Xue, and X. C. Ma, Direct observation of high-temperature superconductivity in one-unit-cell FeSe films, Chin. Phys. Lett. **31**, 017401 (2014).

[9] J. G. Guo, S. F. Jin, G. Wang, S. C. Wang, K. X. Zhu, T. T. Zhou, M. He, and X. L. Chen, Superconductivity in the iron selenide $K_xFe_2Se_2$ ($0 \leqslant x \leqslant 1.0$), Phys. Rev. B **82**, 180520(R) (2010).

[10] X. F. Lu, N. Z. Wang, H. Wu, Y. P. Wu, D. Zhao, X. Z. Zeng, X. G. Luo, T. Wu, W. Bao, G. H. Zhang, F. Q. Huang, Q. Z. Huang, and X. H. Chen, Coexistence of superconductivity and antiferromagnetism in $(Li_{0.8}Fe_{0.2})$OHFeSe, Nat. Mater. **14**, 325 (2015).

[11] F.-C. Hsu, J. Luo, K. Yeh, T. Chen, T. Huang, P. Wu, Y. Lee, Y. Huang, Y. Chu, D. Yan, and M. Wu, Superconductivity in the PbO-type structure α-FeSe, Proc. Natl. Acad. Sci. USA **105**, 14262 (2008).

[12] W. Bao, Q. Z. Huang, G. F. Chen, M. A. Green, D. M. Wang, J. B. He, and Y. M. Qiu, A novel large moment antiferromagnetic order in $K_{0.8}Fe_{1.6}Se_2$ superconductor, Chin. Phys. Lett. **28**, 086104 (2011).

[13] F. Chen, M. Xu, Q. Q. Ge, Y. Zhang, Z. R. Ye, L. X. Yang, J. Jiang, B. P. Xie, R. C. Che, M. Zhang, A. F. Wang, X. H. Chen, D. W. Shen, J. P. Hu, and D. L. Feng, Electronic Identification of the Parental Phases and Mesoscopic Phase Separation of $K_xFe_{2-y}Se_2$ Superconductors, Phys. Rev. X **1**, 021020 (2011).

[14] Q. Y. Wang, Z. Li, W. H. Zhang, Z. C. Zhang, J. S. Zhang, W. Li, H. Ding, Y. B. Ou, P. Deng, K. Chang, J. Wen, C. L. Song, K. He, J. F. Jia, S. H. Ji, Y. Y. Wang, L. L. Wang, X. Chen, X. C. Ma, and Q. K. Xue, Interface-induced high-temperature superconductivity in single unit-cell FeSe films on $SrTiO_3$, Chin. Phys. Lett. **29**, 037402 (2012).

[15] J. J. Lee, F. T. Schmitt, R. G. Moore, S. Johnston, Y.-T. Cui, W. Li, M. Yi, Z. K. Liu, M. Hashimoto, Y. Zhang, D. H. Lu, T. P. Devereaux, D.-H. Lee, and Z.-X. Shen, Interfacial mode coupling as the origin of the enhancement of T_c in FeSe films on $SrTiO_3$, Nature (London) **515**, 245 (2014).

[16] F. W. Zheng, Z. G. Wang, W. Kang, and P. Zhang, Antiferromagnetic FeSe monolayer on $SrTiO_3$: The charge doping and electric field effects, Sci. Rep. **3**, 2213 (2013).

[17] T. P. Ying, X. L. Chen, G. Wang, S. F. Jin, T. T. Zhou, X. F. Lai, H. Zhang, and W. Y. Wang, Observation of superconductivity at $30 \sim 46$ K in $A_xFe_2Se_2$ (A = Li, Na, Ba, Sr, Ca, Yb, and Eu), Sci. Rep. **2**, 426 (2012).

[18] E.-W. Scheidt, V. R. Hathwar, D. Schmitz, A. Dunbar, W. Scherer, F. Mayr, V. Tsurkan, J. Deisenhofer, and A. Loidl, Superconductivity at $T_c = 44$ K in $Li_xFe_2Se_2(NH_3)_y$, Eur. Phys. J. B **85**, 279 (2012).

[19] T. P. Ying, X. L. Chen, G. Wang, S. F. Jin, X. F. Lai, T. T. Zhou, H. Zhang, S. J. Shen, and W. Y. Wang, Superconducting phases in potassium-intercalated iron selenides, J. Am. Chem. Soc. **135**, 2951 (2013).

[20] M. Burrard-Lucas, D. G. Free, S. J. Sedlmaier, J. D. Wright, S. J. Cassidy, Y. Hara, A. J. Corkett, T. Lancaster, P. J. Baker, S. J. Blundell, and S. J. Clarke, Enhancement of the superconducting transition temperature of FeSe by intercalation of a molecular spacer layer, Nat. Mater. **12**, 15 (2013).

[21] S. J. Sedlmaier, S. J. Cassidy, R. G. Morris, M. Drakopoulos, C. Reinhard, S. J. Moorhouse, D. O'Hare, P. Manuel, D. Khalyyavin, and S. J. Clarke, Ammonia-rich high-temperature superconducting intercalates of iron selenide revealed through time-resolved in situ x-ray and neutron diffraction, J. Am. Chem. Soc. **136**, 630 (2014).

[22] H. C. Lei, J. G. Guo, F. Hayashi, and H. Hosono, Emergence of magnetism and controlling factors of superconductivity in Li/Na-ammonia cointercalated $FeSe_{1-z}Te_z$, Phys. Rev. B **90**, 214508 (2014).

[23] See Supplemental Material at http://link.aps.org/supplemental/10.1103/PhysRevB.96.064512 for characterization of FeSe single crystals, the powder XRD pattern of LiFeSe-122, $\rho_c(T)$ curves for several crystals, and the angular dependence of $\rho_{ab}(\theta, \mu_0 H)$ at various temperatures.

[24] X. Dong, K. Jin, D. Yuan, H. Zhou, J. Yuan, Y. Huang, W. Hua, J. Sun, P. Zheng, W. Hu, Y. Mao, M. Ma, G. Zhang, F. Zhou, and Z. Zhao, $(Li_{0.84}Fe_{0.16})OHFe_{0.98}Se$ superconductor: Ion-exchange synthesis of large single-crystal and highly two-dimensional electron properties, Phys. Rev. B **92**, 064515 (2015).

[25] H.-S. Lee, M. Bartkowiak, J.-H. Park, J.-Y. Lee, J.-Y. Kim, N.-H. Sung, B. K. Cho, C.-U. Jung, J. S. Kim, and H.-J. Lee, Effects of two gaps and paramagnetic pair breaking on the upper critical field of $SmFeAsO_{0.85}$ and $SmFeAsO_{0.8}F_{0.2}$ single crystals, Phys. Rev. B **80**, 144512 (2009).

[26] J. A. Fendrich, W. K. Kwok, J. Giapintzakis, C. J. van der Beck, V. M. Vinokur, S. Fleshier, U. Welp, H. K. Viswanathan, and G. W. Crabtree, Vortex Liquid State in an Electron Irradiated Untwinned $YBa_2Cu_3O_{7-\delta}$ Crystal, Phys. Rev. Lett. **74**, 1210 (1995).

[27] N. R. Werthamer, E. Helfand, and P. C. Hohenberg, Temperature and purity dependence of the superconducting critical field, H_{c2}. III. electron spin and spin-orbit effects, Phys. Rev. **147**, 295 (1966).

[28] G. Blatter, M. V. Feigel'man, V. B. Geshkenbein, A. I. Larkin, and V. M. Vinokur, Vortices in high-temperature superconductors, Rev. Mod. Phys. **66**, 1125 (1994).

[29] S. I. Vedeneev, B. A. Piot, D. K. Maude, and A. V. Sadakov, Temperature dependence of the upper critical field of FeSe single crystals, Phys. Rev. B **87**, 134512 (2013).

[30] M. Abdel-Hafiez, Y.-Y. Zhang, Z.-Y. Cao, C.-G. Duan, G. Karapetrov, V. M. Pudalov, V. A. Vlasenko, A. V. Sadakov, D. A. Knyazev, T. A. Romanova, D. A. Chareev, O. S. Volkova, A. N. Vasiliev, and X.-J. Chen, Superconducting properties of sulfur-doped iron selenide, Phys. Rev. B **91**, 165109 (2015).

[31] F. Hunte, J. Jaroszynski, A. Gurevich, D. C. Larbalestier, R. Jin, A. S. Sefat, M. A. McGuire, B. C. Sales, D. K. Christen, and D. Mandrus, Two-band superconductivity in $LaFeAsO_{0.89}F_{0.11}$ at very high magnetic fields, Nature (London) **453**, 903 (2008).

[32] H. Q. Yuan, J. Singleton, F. F. Balakirev, S. A. Baily, G. F. Chen, J. L. Luo, and N. L. Wang, Nearly isotropic superconductivity in $(Ba,K)Fe_2As_2$, Nature (London) **457**, 565 (2009).

[33] H. C. Lei, K. F. Wang, R. Hu, H. Ryu, M. Abeykoon, E. S. Bozin, and C. Petrovic, Iron chalcogenide superconductors at high magnetic fields, Sci. Technol. Adv. Mater. **13**, 054305 (2012).

[34] X. Yi, C. Wang, Q. Tang, T. Peng, Y. Qiu, J. Xu, H. Sun, Y. Luo, and B. Yu, Vortex phase transition and anisotropy behavior of optimized ($Li_{1-x}Fe_xOH$)FeSe single crystals, Supercond. Sci. Technol. **29**, 105015 (2016).

[35] D. Guterding, H. O. Jeschke, P. J. Hirschfeld, and R. Valentí, Unified picture of the doping dependence of superconducting transition temperatures in alkali metal/ammonia intercalated FeSe, Phys. Rev. B **91**, 041112(R) (2015).

[36] J.-L. Zhang, L. Jiao, Y. Chen, and H.-Q. Yuan, Universal behavior of the upper critical field in iron-based superconductors, Front. Phys. **6**, 463 (2011).

[37] A. P. Pippard, *Magnetoresistance in Metals* (Cambridge University Press, Cambridge, 1993).

[38] R. H. McKenzie, J. S. Qualls, S. Y. Han, and J. S. Brooks, Violation of Kohler's rule by the magnetoresistance of a quasi-two-dimensional organic metal, Phys. Rev. B **57**, 11854 (1998).

[39] B. Lei, J. H. Cui, Z. J. Xiang, C. Shang, N. Z. Wang, G. J. Ye, X. G. Luo, T. Wu, Z. Sun, and X. H. Chen, Evolution of High-Temperature Superconductivity from a Low-T_c Phase Tuned by Carrier Concentration in FeSe Thin Flakes, Phys. Rev. Lett. **116**, 077002 (2016).

[40] M. D. Watson, T. Yamashita, S. Kasahara, W. Knafo, M. Nardone, J. Béard, F. Hardy, A. McCollam, A. Narayanan, S. F. Blake, T. Wolf, A. A. Haghighirad, C. Meingast, A. J. Schofield, H. v. Löhneysen, Y. Matsuda, A. I. Coldea, and T. Shibauchi, Dichotomy between the Hole and Electron Behavior in Multiband Superconductor FeSe Probed by Ultrahigh Magnetic Fields, Phys. Rev. Lett. **115**, 027006 (2015).

[41] C. M. Hurd, *Hall Effect in Metals and Alloys* (Plenum, New York, 1972).

[42] V. Brouet, P. H. Lin, Y. Texier, J. Bobroff, A. Taleb-Ibrahimi, P. L. Fèvre, F. Bertran, M. Casula, P. Werner, S. Biermann, F. Rullier-Albenque, A. Forget, and D. Colson, Large Temperature Dependence of the Number of Carriers in Co-Doped $BaFe_2As_2$, Phys. Rev. Lett. **110**, 167002 (2013).

[43] A. F. Wang, J. J. Ying, X. G. Luo, Y. J. Yan, D. Y. Liu, Z. J. Xiang, P. Cheng, G. J. Ye, L. J. Zou, Z. Sun, and X. H. Chen, A crossover in the phase diagram of $NaFe_{1-x}Co_xAs$ determined by electronic transport measurements, New J. Phys. **15**, 043048 (2013).

[44] I. I. Mazin, Symmetry analysis of possible superconducting states in $K_xFe_ySe_2$ superconductors, Phys. Rev. B **84**, 024529 (2011).

[45] M. Khodas and A. V. Chubukov, Interpocket Pairing and Gap Symmetry in Fe-Based Superconductors with Only Electron Pockets, Phys. Rev. Lett. **108**, 247003 (2012).

[46] N. Hao and J. Hu, Odd parity pairing and nodeless antiphase $s^{\pm}$ in iron-based superconductors, Phys. Rev. B **89**, 045144 (2014).

[47] E. M. Nica, R. Yu, and Q. Si, Orbital selective pairing and superconductivity in iron selenides, npj Quant. Mater. **2**, 24 (2017).

[48] B. Lei, Z. J. Xiang, X. F. Lu, N. Z. Wang, J. R. Chang, C. Shang, A. M. Zhang, Q. M. Zhang, X. G. Luo, T. Wu, Z. Sun, and X. H. Chen, Gate-tuned superconductor-insulator transition in (Li, Fe)OHFeSe, Phys. Rev. B **93**, 060501(R) (2016).

[49] J. He, X. Liu, W. Zhang, L. Zhao, D. Liu, S. He, D. Mou, F. Li, C. Tang, Z. Li, L. Wang, Y. Peng, Y. Liu, C. Chen, L. Yu, G. Liu, X. Dong, J. Zhang, C. Chen, Z. Xu, X. Chen, X. Ma, Q. Xue, and X. J. Zhou, Electronic evidence of an insulator-superconductor crossover in single-layer $FeSe/SrTiO_3$ films, Proc. Natl. Acad. Sci. USA **111**, 18501 (2014).

[50] T. Hatakeda, T. Noji, K. Sato, T. Kawamata, M. Kato, and Y. Koike, New alkali-metal- and 2-phenethylamine-intercalated superconductors $A_x(C_8H_{11}N)_yFe_{1-z}Se_2$ (A = Li, Na) with the largest interlayer spacings and $T_c \sim 40$ K, J. Phys. Soc. Jpn. **85**, 103702 (2016).

[51] C. H. P. Wen, H. C. Xu, C. Chen, Z. C. Huang, X. Lou, Y. J. Pu, Q. Song, B. P. Xie, M. Abdel-Hafiez, D. A. Chareev, A. N. Vasiliev, R. Peng, and D. L. Feng, Anomalous correlation effects and unique phase diagram of electron-doped FeSe revealed by photoemission spectroscopy, Nat. Commun. **7**, 10840 (2016).

[52] T. Noji, T. Hatakeda, S. Hosono, T. Kawamata, M. Kato, and Y. Koike, Synthesis and post-annealing effects of alkaline-metal-ethylenediamineintercalated superconductors $A_x(C_2H_8N_2)_yFe_{2-z}Se_2$ (A = Li, Na) with $T_c = 45$ K, Phys. C (Amsterdam, Neth.) **504**, 8 (2014).

[53] T.-K. Chena, C.-C. Changa, H.-H. Changb, A.-H. Fanga, C.-H. Wanga, W.-H. Chaoa, C.-M. Tsenga, Y.-C. Leea, Y.-R. Wua, M.-H. Wena, H.-Y. Tangd, F.-R. Chena, M.-J. Wanga, M.-K. Wua, and D. V. Dyck, Fe-vacancy order and superconductivity in tetragonal β-$Fe_{1-x}Se$, Proc. Natl. Acad. Sci. USA **111**, 63 (2014).

[54] C.-H. Wang, T.-K. Chen, C.-C. Chang, C.-H. Hsu, Y.-C. Lee, M.-J. Wang, P. M. Wu, and M.-K. Wu, Disordered Fe vacancies and superconductivity in potassium-intercalated iron selenide ($K_{2-x}Fe_{4+y}Se_5$), Europhys. Lett. **111**, 27004 (2015).

[55] T. Berlijn, P. J. Hirschfeld, and W. Ku, Effective Doping and Suppression of Fermi Surface Reconstruction via Fe Vacancy Disorder in $K_xFe_{2-y}Se_2$, Phys. Rev. Lett. **109**, 147003 (2012).

[56] A.-M. Zhang, T.-L. Xia, K. Liu, W. Tong, Z. R. Yang, and Q.-M. Zhang, Superconductivity at 44 K in K intercalated FeSe system with excess Fe, Sci. Rep. **3**, 1216 (2013).

[57] J. P. Sun, G. Z. Ye, P. Shahi, J.-Q. Yan, K. Matsuura, H. Kontani, G. M. Zhang, Q. Zhou, B. C. Sales, T. Shibauchi, Y. Uwatoko, D. J. Singh, and J.-G. Cheng, High-T_c Superconductivity in FeSe at High Pressure: Dominant Hole Carriers and Enhanced Spin Fluctuations, Phys. Rev. Lett. **118**, 147004 (2017).